



A naphthalene-quinoline based chemosensor for fluorescent “turn-on” and absorbance-ratiometric detection of Al³⁺ and its application in cells imaging

Shuang Zeng^{a,1}, Shi-Jie Li^{b,1}, Xue-Jiao Sun^a, Ming-Qiang Li^a, Yu-Qing Ma^a, Zhi-Yong Xing^{a,*}, Jin-Long Li^c

^a Department of Applied Chemistry, College of Science, Northeast Agricultural University, Harbin 150030, PR China

^b College of Animal Science and Technology, Northeast Agricultural University, Harbin 150030, PR China

^c School of Chemistry and Chemical Engineering, Qiqihar University, Qiqihar 161006, PR China

ARTICLE INFO

Article history:

Received 12 April 2018

Received in revised form 11 July 2018

Accepted 12 July 2018

Available online xxx

Keywords:

Naphthalene

Quinoline

Chemosensor

Ratiometric

Cells HSC

ABSTRACT

A new naphthalene-quinoline based chemosensor **L** was prepared and structurally characterized. **L** exhibited excellent selectivity and sensitivity to Al³⁺ through distinct fluorescence enhancement (335-fold) and ratiometric detection in DMF/H₂O (v/v, 1/9) based on the combined mechanisms of ESIPT and CHEF. The recognizing behavior of **L** toward Al³⁺ had been investigated in detail through Job's Plot, FT-IR, HNMR, and HRMS analysis. The limit of detection (LOD) for Al³⁺ was as low as and 3.67×10^{-8} M. **L** was successfully applied in real sample detection and construction of molecular logic gate. Moreover, **L** was verified to be of low cytotoxicity and good imaging characteristics for the detection of Al³⁺ in cells HSC.

© 2018 Elsevier B.V. All rights reserved.

1. Introduction

Aluminum, the third most abundant metal in the earth's crust (approximately 8% of total mineral components) [1–4], is closely related to people's lives due to its widely use in food additives, cooking utensils, paper and packing materials, textile, clinical drugs and water treatment [5–7]. However, as non-essential element for human, accumulation of excessive amount of Al³⁺ can cause a number of diseases such as Parkinson's disease, Alzheimer's disease, amyotrophic lateral sclerosis, anemia, liver damages and hemochromatosis [8–11]. Furthermore, high concentration of Al³⁺ can hamper plant growth and kill fish in aquatic ecosystems [12,13]. According to the recommendation of world health organization (WHO), average human intake capacity of aluminum is 3–10 mg/day and the permitted level of Al³⁺ in drinking water is 7.4 μM [14]. Thus, the design of chemosensors for detecting Al³⁺ in aqueous medium is of great significance.

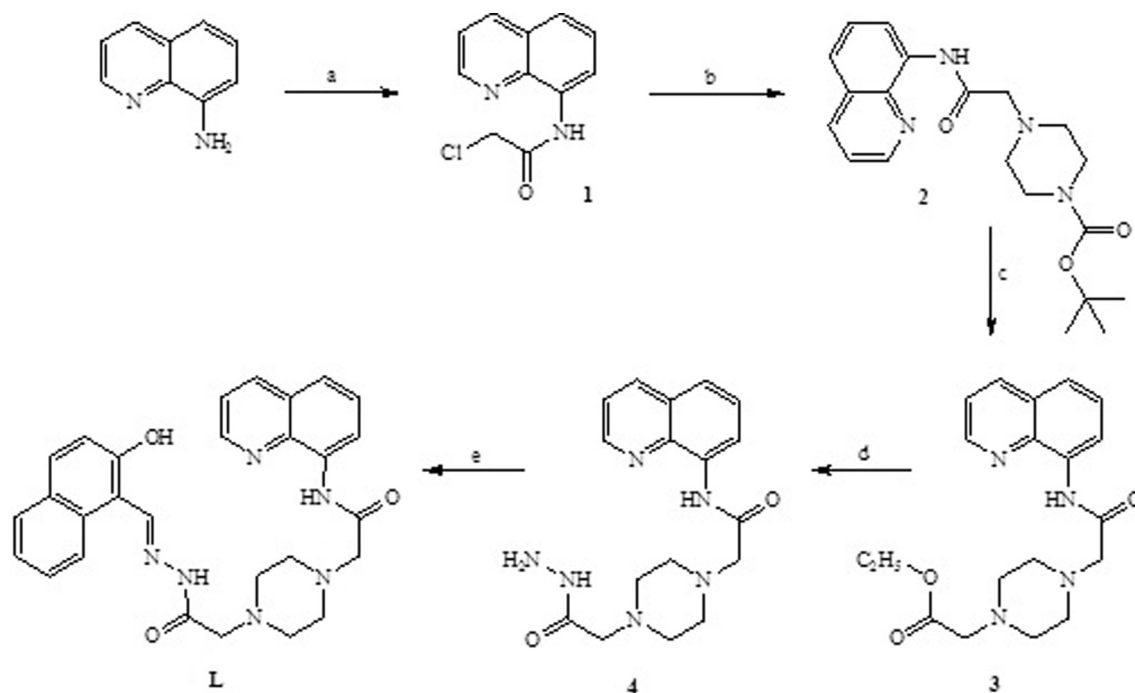
Over the past few decades, many modern techniques were employed for the detection of Al³⁺, such as classical atomic absorption spectrometry, inductively coupled plasma mass spectroscopy, electrochemical methods, hydride generation-atomic, neutron activation analysis and ion chromatography [15–18]. Compared with those detection

methods mentioned above, fluorescence detection method has drawn special attention of the researchers attribute to its simple and convenient operation, high selectivity and sensitivity, rapidity, non-destructive and naked-eye recognition [12,19–22]. However, it is still difficult to design a sensitive and selective fluorescent chemosensor for Al³⁺ due to its drawbacks such as lack of spectroscopic characteristics, poor coordination and strong hydration ability [23]. Moreover, compared with the intensity-based probes [12,24–28], ratiometric sensing of an analyte is gaining more and more attention because the ratio of two intensities of absorption or emission wavelength reduces the error (s) which could have been arising from the physical and chemical method. A number of ratiometric Al³⁺ sensors based on various fluorophores and sensing mechanisms have been developed [29–36], but some of them still suffer from the shortcomings such as complicated synthesis, insolubility in water, or interfered by other trivalent metal ion such as Fe³⁺ and Cr³⁺ and lack practical applicability in real samples. Moreover, to our best knowledge, there were few papers concerning the fluorogenic and ratiometric absorbance chemosensor for Al³⁺ based on naphthalene-quinoline [33]. In order to extend our research on the development of Al³⁺ chemosensor [37–39], as show in Scheme 1, we designed and synthesized a novel naphthalene-quinoline chemosensor **L**. **L** showed excellent selectivity and sensitivity to Al³⁺ through fluorescence enhancement (335-fold) and ratiometric absorption detection in DMF/H₂O (v/v, 1/9). Furthermore, the chemosensor **L** was successfully applied in detection of Al³⁺ in real water samples and the fluorescence signal of chemosensor **L** could be

* Corresponding author.

E-mail address: zyxing@neau.edu.cn (Z.-Y. Xing).

¹ These authors contributed equally to this work and should be considered co-first authors.



Scheme 1. Synthesis of sensor L. Reagents and conditions: (a) dichloromethane, chloroacetyl chloride, triethylamine, reflux; (b) 1-boc-piperazine, K_2CO_3 , acetonitrile, reflux; (c) acetonitrile, K_2CO_3 , HCl, Ethyl bromoacetate, reflux; (d) hydrazine hydrate, CH_3OH , reflux; (e) CH_3OH , 2-Hydroxy-1-naphthaldehyde, reflux.

used in the construction of molecular logic gate. We also found that the application of **L** for the imaging of Al^{3+} in human stromal cell (HSC) by fluorescence changes was also achieved.

2. Experimental

2.1. Materials and Instruments

Unless otherwise specified, all the solvents and reagents (analytical or spectroscopic grade) were obtained commercially and used without further purification. 1H NMR spectra and ^{13}C NMR spectra were recorded on a Bruker AV-600 spectrometer. Chemical shifts (δ) are reported in ppm, relative to TMS (tetramethylsilane) and using $DMSO-d_6$ as the solvent. UV-vis spectroscopy measurements were acquired on a Pgeneral TU-1901 and absorption spectra were recorded at 25 °C. Fluorescence measurements were measured on a Perkin Elmer LS55 fluorescence spectrometer. Mass spectra were measured on a Waters Xevo UPLC/G2-SQ ToF MS spectrometer. The melting point was measured on a Beijing XT4-100X microscopic melting point apparatus. The pH measurements were made with a model PHS-3C meter (Shanghai, China). Cell image were collected using laser confocal microscope (Leica, TCS SP2 AOBS).

2.2. Synthesis

The intermediate compounds **1–4** were prepared according to the reported procedure [39–41].

2.2.1. Synthesis of Intermediate Compound 1

In a 100 mL round bottom flask equipped with dichloromethane (10 mL), 8-aminoquinoline (580 mg, 4 mmol) and TEA (0.3 mL) were added successively. Chloroacetyl chloride (0.15 mL) dissolved in dichloromethane (10 mL) was slowly added to a round bottom flask with a dropping funnel. The solution was stirred at room temperature for 24 h. After the complete consumption of the starting material monitored using TLC, the mixture was extracted with hydrochloric acid (1 M, 20 mL) three times. The dichloromethane layers were dried with anhydrous sodium sulfate and evaporated under vacuum. The

crude product was purified by column chromatography on silica gel using dichloromethane as eluent to get white needle-like solid **1** (600 mg, yield: 68.1%); m.p.:148–149 °C. 1H NMR (600 MHz, $DMSO-d_6$) δ (ppm) 10.71 (s, 1H), 9.00–8.93 (m, 1H), 8.65 (d, $J = 7.7$ Hz, 1H), 8.45 (d, $J = 8.3$ Hz, 1H), 7.74 (d, $J = 8.2$ Hz, 1H), 7.68 (dd, $J = 8.2, 4.2$ Hz, 1H), 7.63 (t, $J = 8.0$ Hz, 1H), 4.63 (s, 2H).

2.2.2. Synthesis of Intermediate Compound 2

The 1-boc-piperazine (450 mg, 2.4 mmol) and K_2CO_3 (500 mg, 3.6 mmol) were added to a stirred solution of compound **1** (440 mg, 2 mmol) in acetonitrile (30 mL) and refluxed for 6 h. After the complete consumption of the starting material monitored using TLC, the reaction mixture was allowed to room temperature and the solvent was removed under reduced pressure. The crude product was purified by column chromatography on silica gel using $MeOH/CH_2Cl_2$ (v/v, 1/20) to get white solid **2** (520 mg, yield: 70.2%); m.p.:165–166 °C. 1H NMR (600 MHz, $DMSO-d_6$) δ (ppm) 11.30 (s, 1H), 8.97–8.90 (m, 1H), 8.63 (d, $J = 7.6$ Hz, 1H), 8.39 (d, $J = 8.3$ Hz, 1H), 7.66 (d, $J = 8.2$ Hz, 1H), 7.62 (dd, $J = 8.2, 4.2$ Hz, 1H), 7.57 (t, $J = 7.9$ Hz, 1H), 3.48 (s, 4H), 3.27 (s, 2H), 2.54 (m, 4H), 1.40 (s, 9H).

2.2.3. Synthesis of Intermediate Compound 3

The compound **2** (550 mg, 1.5 mmol) and hydrochloric acid (1 M, 3 mL) were dissolved in acetonitrile (20 mL), and the reaction mixture was allowed to reflux for 2 h. After cooling to the room temperature, ethyl bromoacetate (250 mg, 1.5 mmol) and K_2CO_3 (1.38 g, 10 mmol) were directly added to the mixture and refluxed for 5 h. The reaction mixture was cooled and solvent was evaporated under reduced pressure. The crude product was purified by column chromatography on silica gel using $MeOH/CH_2Cl_2$ (v/v, 1/30) to get compound **3** as yellow oil liquid (336 mg, yield: 63%). 1H NMR (600 MHz, $DMSO-d_6$) δ (ppm) 11.36 (s, 1H), 8.95 (dd, $J = 4.2, 1.6$ Hz, 1H), 8.65 (dd, $J = 7.6, 1.2$ Hz, 1H), 8.41 (dd, $J = 8.3, 1.6$ Hz, 1H), 7.68–7.64 (m, 2H), 7.59 (t, $J = 7.9$ Hz, 1H), 4.13 (q, $J = 7.1$ Hz, 2H), 3.31 (s, 2H), 3.26 (s, 2H), 2.72 (s, 4H), 2.63 (s, 4H), 1.23 (t, $J = 7.1$ Hz, 3H).

2.2.4. Synthesis of Intermediate Compound 4

The compound **3** (180 mg, 0.5 mmol) and hydrazine hydrate (100 mg, 2 mmol) were dissolved in methanol (20 mL). Then the

mixture was refluxed for 2 h under stirring. After completion of reaction as checked by TLC, the solvent was removed under reduced pressure. The crude product was purified by column chromatography on silica gel using MeOH/CH₂Cl₂ (v/v, 1/20) to get white solid **4** (154 mg, yield: 90%); m.p.: 194–196 °C. ¹H NMR (600 MHz, DMSO *d*₆) δ (ppm) 11.32 (s, 1H), 8.93 (d, *J* = 2.8 Hz, 1H), 8.90 (s, 1H), 8.62 (d, *J* = 7.3 Hz, 1H), 8.39 (d, *J* = 8.2 Hz, 1H), 7.69–7.59 (m, 2H), 7.57 (t, *J* = 7.9 Hz, 1H), 4.23 (s, 2H), 3.23 (s, 2H), 2.98 (s, 2H), 2.61 (s, 8H).

2.2.5. Synthesis of Sensor **L**

The compound **4** (102 mg, 0.3 mmol) and 2-hydroxy-1-naphthaldehyde were dissolved in methanol (20 mL). The reaction mixture was refluxed 2 h. After the complete consumption of the starting material monitored using TLC, the reaction mixture was cooled to room temperature. The precipitate was filtered and washed 5 times with ethanol to get the yellow product **L** (100 mg, yield 69%); m.p.: 262–263 °C. ¹H NMR (600 MHz, DMSO *d*₆) (Fig. S1) δ (ppm) 12.74 (s, 1H), 11.49 (s, 1H), 11.38 (s, 1H), 9.45 (s, 1H), 8.95 (d, *J* = 1.5 Hz, 1H), 8.63 (d, *J* = 7.6 Hz, 1H), 8.39 (d, *J* = 8.3 Hz, 1H), 8.22 (d, *J* = 8.7 Hz, 1H), 7.91 (d, *J* = 8.9 Hz, 1H), 7.88 (d, *J* = 8.3 Hz, 1H), 7.65 (d, *J* = 8.2 Hz, 1H), 7.62–7.54 (m, 3H), 7.39 (t, *J* = 7.4 Hz, 1H), 7.21 (d, *J* = 8.9 Hz, 1H), 3.32 (s, 2H), 3.27 (s, 2H), 2.72 (s, 8H). ¹³C NMR (151 MHz, DMSO *d*₆) (Fig. S2) δ (ppm) 169.05, 165.96, 158.33, 149.72, 147.03, 138.38, 136.98, 134.39, 133.01, 132.11, 129.35, 128.33, 128.24, 127.48, 122.67, 121.32, 119.36, 115.86, 108.97, 62.10, 60.98, 53.66, 53.02. HRMS *m/z* (TOF MS ES⁺) (Fig. S3): calcd for C₂₈H₂₉N₆O₃: 497.2301[M + H]⁺, found: 497.2306.

2.3. General Procedures of Spectral Detection

2.3.1. Preparation of Stock Solutions

Stock solution of **L** (0.1 mM) was prepared with pure DMF and 50 mL of **L** solution (0.1 mM) was diluted in 450 mL ultrapure water to make the final concentration of 10 μM. Stock solutions of metal ions (10 mM) were prepared in ultrapure water using NaClO₄, KClO₄, Mg(ClO₄)₂, Ba(ClO₄)₂, Zn(ClO₄)₂·6H₂O, Cu(ClO₄)₂·6H₂O, AgNO₃, Cd(NO₃)₂, Pb(NO₃)₂, Co(NO₃)₂·6H₂O, Ni(NO₃)₂·6H₂O, Fe(ClO₄)₃·xH₂O, Ca(NO₃)₂·4H₂O, Al(NO₃)₃·9H₂O, MnSO₄·H₂O, HgCl₂, and FeCl₂·4H₂O.

2.3.2. Fluorescence and UV–Vis Absorption Selectivity Experiments

In the fluorescence and UV–vis absorption selectivity experiments, different metal ions (Na⁺, K⁺, Mg²⁺, Ba²⁺, Zn²⁺, Cu²⁺, Ag⁺, Cd²⁺, Pb²⁺, Co²⁺, Ni²⁺, Fe²⁺, Fe³⁺, Ca²⁺, Al³⁺, Mn²⁺, Hg²⁺) (each of 5

equiv.) were individually added into the **L** (10 μM) solution, the fluorescence and UV–vis absorption spectrum of each sample were measured, respectively.

2.3.3. Fluorescence Competition Experiments

50 μL of each metal solution (10 mM) were taken and added into 10 mL of each **L** solution (10 μM) prepared above to make 5 equiv. Then, 50 μL of the Al³⁺ solution (10 mM) were added into the mixed solution of each metal ion and **L** to make 5 equiv. Fluorescence spectra were taken at room temperature after mixing them.

2.3.4. Fluorescence and UV–Vis Absorption Titration Experiments

For fluorescence titration, increasing doses of Al³⁺ (0–8 equiv.) were added into **L** (10 μM) solution to give the samples that containing different Al³⁺ concentrations, then the fluorescence spectrum of each sample was measured. For UV–vis absorption titration, a procedure similar to that in fluorescence titration was adopted except that the Al³⁺ was used from 0 to 2 equiv.

2.3.5. Job Plot Measurement

A series of DMF/H₂O solution (1/9, v/v) containing **L** and Al³⁺ were prepared so that the total concentration of Al³⁺ and **L** was kept as 10 μM. The mole fraction of Al³⁺ was varied from 0.1 to 0.9. Fluorescence spectra were taken at room temperature.

2.4. Preparation of [L–Al³⁺]

The compound **L** (10 mg, 0.02 mmol) and Al(NO₃)₃·9H₂O (7.5 mg, 0.02 mmol) were dissolved in ethanol (10 mL). Then the mixture was refluxed for 2 h under stirring. The solution turned to deep yellow and cooled to the temperature. After removing the solvent under reduced pressure and drying under vacuum for 60 min, the **L**–Al³⁺ complex (yellow solid) were obtained and directly used for spectrum measurement without further purification.

2.5. Cell Culture and Staining

The human stromal cell line (HSC) purchased from ATCC (CRL-4003) was routinely cultured in 1:1 mixture of DMEM medium and F-12 medium supplemented with 10% heat-inactivated FBS, 100 U/mL penicillin, 100 μg/mL streptomycin, and 1 mM sodium pyruvate at 37 °C, 5%CO₂ for maintained. After plant HSC into 35 mm

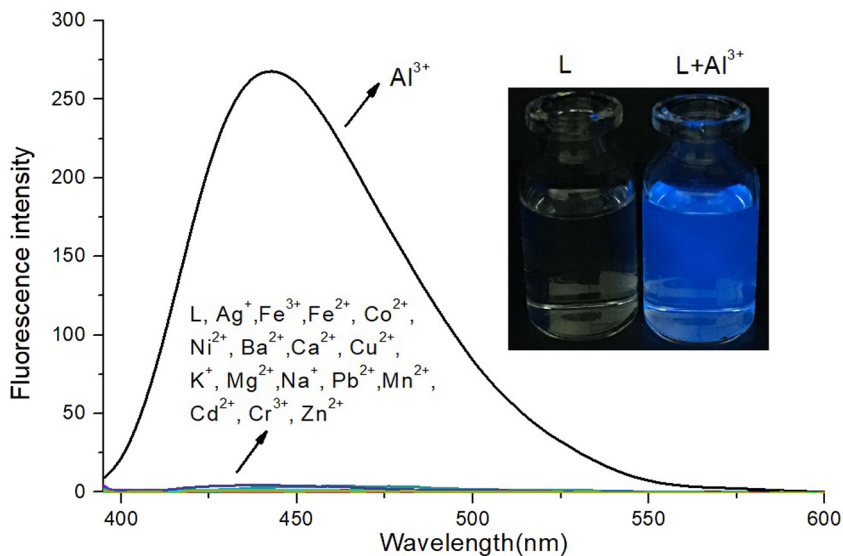
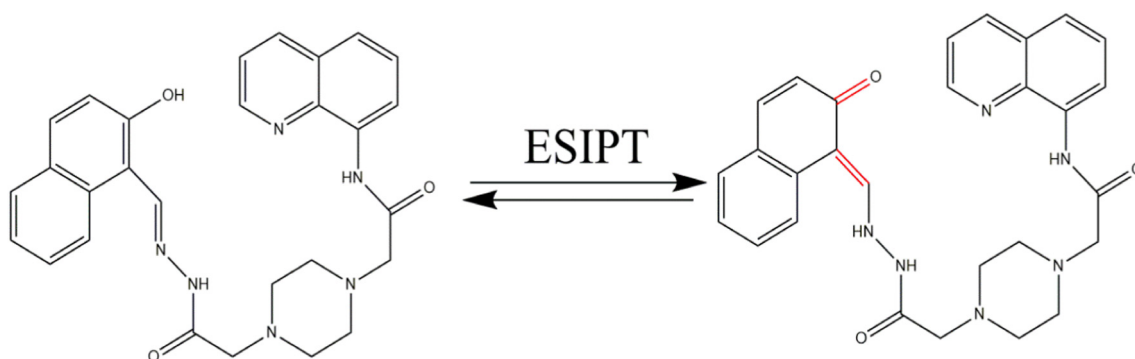


Fig. 1. Fluorescence emission spectra ($\lambda_{\text{exc}} = 380 \text{ nm}$) of **L** (10 μM) in the presence of 5 equiv. of various metal ions in DMF/H₂O (1/9, v/v). Inset: the color changes of **L** (10 μM) in the presence of Al³⁺ ions (5 equiv.) in DMF/H₂O (1/9, v/v) under UV light of 365 nm.



Scheme 2. Probable one-way ESIPT of sensor **L**.

plates at concentration of 5×10^4 cells/cm², the media without FBS or antibiotic, was used for culture cells and chemical treatment. There were three **L** staining groups: A. normal group: HSC were not treated with Al(NO₃)₃; B. low concentration group: HSC were incubated 1 h with 1 mL media added Al(NO₃)₃ (5×10^{-6} M); C. high concentration group: HSC were incubated 1 h with 1 mL media added Al(NO₃)₃ (5×10^{-5} M). Then fibroblast cells of every group were washed with PBS 3 times and were fixed by using a standard paraformaldehyde fixation protocol. After fixation, fibroblast cells were rinsed with 4:6 mixture solution of DMF and water and then stained by incubating for 2 h with **L** (1×10^{-4} M). Lastly, the cells were mounted in standard mounting media and imaged by laser confocal microscope, with an excitation wavelength of 405 nm and an emission wavelength of 440 nm.

3. Results and Discussion

The chemosensor **L** was synthesized by the following steps depicted in Scheme 1, and the structure of **L** was fully characterized by ¹HNMR, ¹³CNMR and HRMS analysis.

3.1. Fluorescence Spectra Characteristics for Ions

The fluorescence responses of **L** to various cations were illustrated in Fig. 1. **L** (10 μM) alone exhibited very weak fluorescence-emission ($\lambda_{em} = 440$ nm) in the solution of DMF/H₂O (1/9, v/v). The weak emission of **L** could be attributed to the following two aspects. Firstly, the isomerization of C=N moiety, which can greatly quench the fluorescence of **L** at the excited state. Secondly, the possible one-way ESIPT process of **L** at the excited state (Scheme 2), which leads to nonradiative decay of the excited state and thus caused fluorescence quenching [6,28–30]. However, upon the addition of Al³⁺, a 335-fold fluorescence enhancement was observed at 440 nm, and the solution of **L** showed a significant color change from colorless to bright blue at the same time, which could easily be detected by the naked-eye under UV light of 365 nm. This result was due to chelating of the probe **L** with Al³⁺, which not only inhibited the C=N isomerization and ESIPT processes, but also increased the rigidity of the molecular assembly by restricting the free rotations of the azomethine carbon linking to the naphthalene ring resulting in a significant enhancement of the fluorescence intensity, which is known as chelation-enhanced fluorescence (CHEF). The fluorescent behavior of **L** (10 μM) upon addition of other metal ions like Na⁺, K⁺, Ca²⁺, Mg²⁺, Pb²⁺, Cu²⁺, Co²⁺, Cd²⁺, Ni²⁺, Fe²⁺, Hg²⁺, Mn²⁺, Ag⁺ and Zn²⁺ (50 μM) in DMF/H₂O (1/9, v/v) was also studied but there was hardly any change in emission intensity of **L**. This result shows that the probe **L** has a good selectivity for the identification of Al³⁺.

To better understand the chromaticity changes in fluorescence spectra of the probe **L** upon complexation, CIE chromaticity coordinates

were also calculated from the emission spectrum [42]. The CIE system is a two-dimensional space (XY plane), each point on the chromaticity diagram represents a certain color. The CIE chromaticity coordinates of **L**-Al³⁺ complex was found to be $x = 0.1459$, $y = 0.0777$ at room temperature. This indicates that the color coordinates shifts gradually from navy blue to blue color region upon progressive addition of Al³⁺ into the solution of **L** (Fig. 2).

Moreover, to further reveal the identification performance of **L** to aluminum ions, the titration experiments of **L** with Al³⁺ were done and the results were shown in Fig. 3. Upon the addition of Al³⁺ (0–8equiv.) to **L**, the fluorescence intensity of **L** increases gradually and almost do not change when the addition of Al³⁺ is 4 equivalents. The concentration of aluminum ions shows a good linear relationship with the fluorescence intensity of **L** in the range of 0.1–40 μM (Fig. S4), and the limit of detection (LOD) was calculated as 1.92×10^{-7} M (based on $3\sigma/k$, where σ is the standard deviation of the blank measurements, and k is the slope of the intensity ratio versus sample concentration plot) [43].

To further determine the selectivity of the probe to aluminum ions in the presence of other cations, we also conducted the competitive

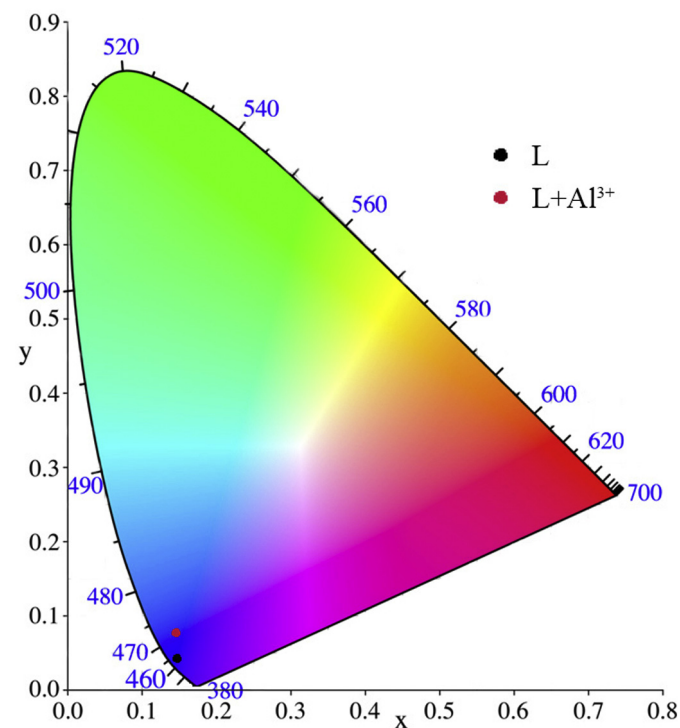


Fig. 2. CIE diagram of the chemosensor **L** and **L** with Al³⁺ (5 equiv.) in DMF/H₂O (1:9 v/v) solution.

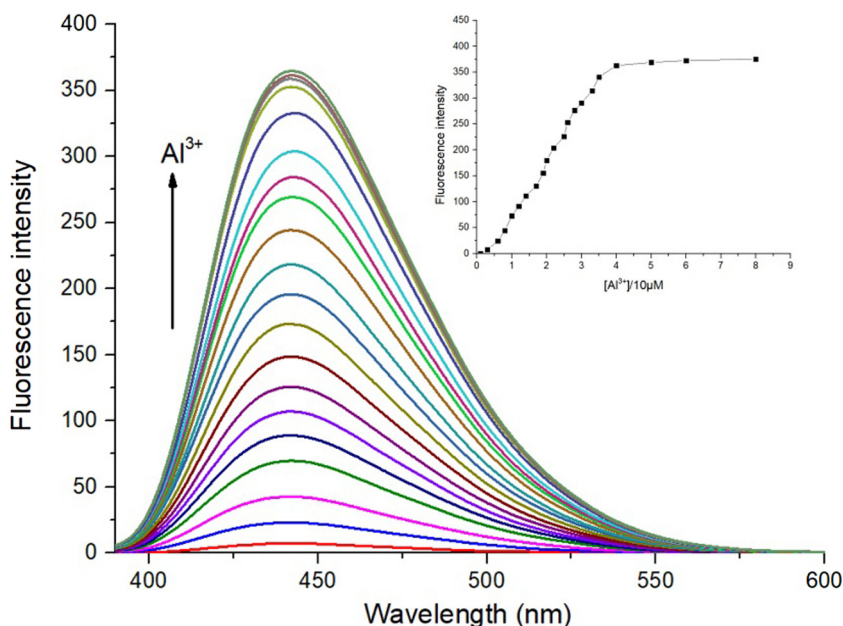


Fig. 3. Fluorescence spectra of **L** (10 μM) on addition of different amount of Al^{3+} in DMF/ H_2O (1/9, v/v). Inset: fluorescence intensity at 440 nm versus the number of equiv. of Al^{3+} added.

experiment on the probe **L** (10 μM) for Al^{3+} (50 μM) mixed with other tested metal ions such as Na^+ , K^+ , Ca^{2+} , Mg^{2+} , Pb^{2+} , Cu^{2+} , Co^{2+} , Cd^{2+} , Ni^{2+} , Fe^{2+} , Hg^{2+} , Mn^{2+} , Ag^+ and Zn^{2+} (50 μM). As show in Fig. 4, the fluorescence intensity of **L**- Al^{3+} complexation is almost unaffected except for Cu^{2+} which almost completely quenched the fluorescence due to the paramagnetic effect from spin-orbit coupling of Cu^{2+} induced the fluorescence quenching [44]. Thus, the probe **L** has good selectivity for Al^{3+} in the presence of most competing metal ions.

3.2. UV-Vis Studies of **L** Toward Al^{3+}

According to the specific fluorescence responses of **L** to Al^{3+} among the tested cations, the UV-vis absorption of **L** (10 μM) were measured in the absence and presence of Al^{3+} (50 μM) in

DMF/ H_2O (1/9, v/v) solution, respectively. As shown in Fig. 5, the absorption spectrum of **L** (10 μM) exhibited two absorption bands at 320 and 354 nm in DMF/ H_2O (1/9, v/v) solution. However, upon addition of Al^{3+} , the absorption band at 354 nm disappeared and a new band at 400 nm was observed, indicated the formation of complexation between **L** and Al^{3+} . Moreover, the binding properties of **L** with Al^{3+} were further studied by UV-vis titration experiments. On the treatment of Al^{3+} (0–1.2 equiv.) to the solution of **L**, as shown in Fig. 6, the absorption band at 354 nm was gradually attenuated accompanied with a drastic increase in the peak at 400 nm. A well isosbestic point was observed at 375 nm, indicating the formation of the **L**- Al^{3+} adduct. And the absorbance intensity ratios of the receptor **L** at 400 nm and 354 nm (A_{400}/A_{354}) increased linearly with the amount of Al^{3+} in the range of 1–7 μM (Fig. S5), indicating a clear ratiometric absorbance response of the probe **L** toward Al^{3+} .

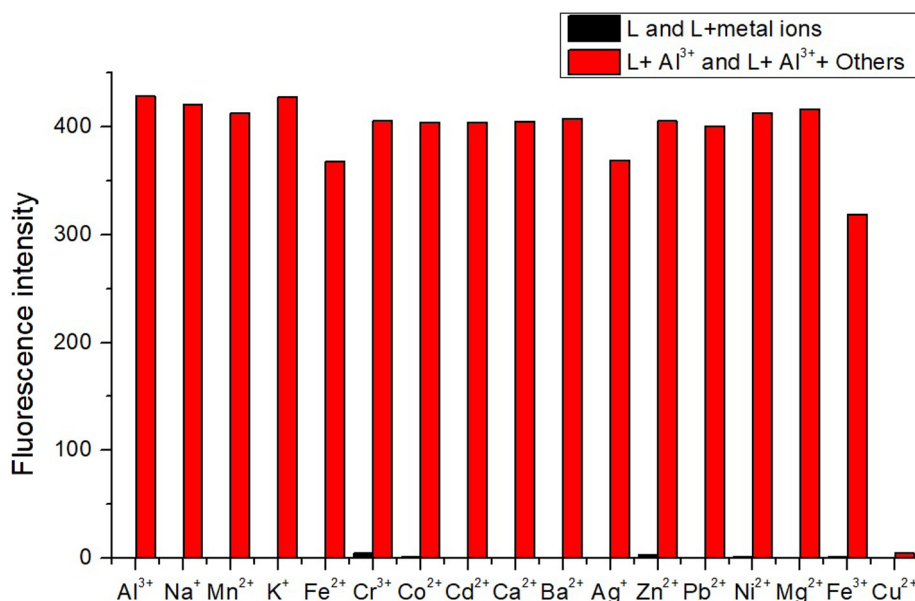


Fig. 4. Competition experiment of receptor **L** toward Al^{3+} in the presence of 5 equiv. of other cations. [**L**] = 10 μM , [Al^{3+}] = 50 μM , and [X^{n+}] = 50 μM in DMF/ H_2O (1/9, v/v). λ_{ex} = 380 nm.

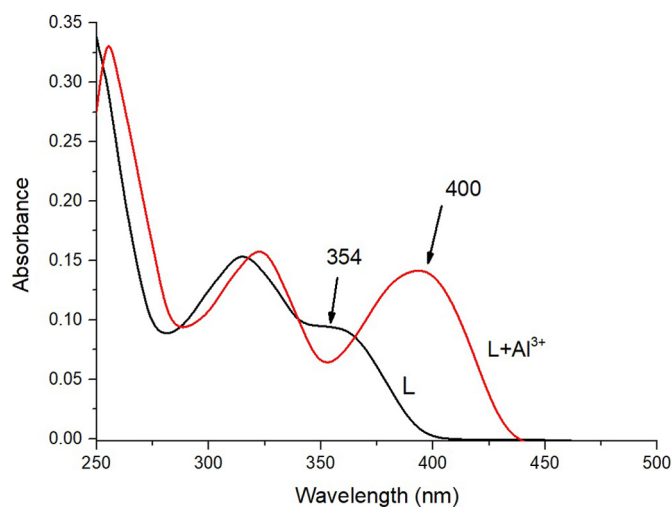


Fig. 5. UV-vis absorption spectra of **L** (10 μM) in the absence (black curve) and presence (red curve) of 5 equiv. of Al^{3+} in DMF/ H_2O (1/9, v/v). (For interpretation of the references to color in this figure legend, the reader is referred to the web version of this article.)

The detection limit was calculated as 3.67×10^{-8} M, which showed that ratiometric detection was more sensitive than that one which calculated from fluorescent titration experiments. The comparative analysis of chemosensor **L** with previously reported sensors were shown in Table 1.

3.3. Binding Stoichiometry and Sensing Mechanism

In order to confirm the binding mechanism of **L** toward Al^{3+} , Job's method for fluorescent titration was carried out (Fig. 7). The maximum fluorescent intensity was reached at a molar fraction of 0.5, which indicate a 1:1 ratio for the **L**- Al^{3+} complex. Furthermore, the ESI mass spectrum of **L**, which is regarded as the direct evidence to study the binding mechanism between cations and the chemosensor, were also measured in the absence and presence of Al^{3+} (Fig. 8). The peaks at m/z 497.2292 and m/z 521.1888 were

attributed to $[\text{L} + \text{H}^+]$ (calcd. m/z 497.2301) and $[\text{L} - 2\text{H} + \text{Al}^{3+}]$ (calcd. m/z 521.1882), respectively, suggesting a 1:1 **L**- Al^{3+} binding stoichiometry, which is consistent with the Job's plot analysis. Based on the Job's plot and ESI-MS analysis, according to the Benesi-Hildebrand plot, the association constant was calculated to be $6.6 \times 10^4 \text{ M}^{-1}$ from nonlinear curve fitting of the absorbance titration data (Fig. S6).

The FT-IR spectra of **L** and **L**- Al^{3+} complexes were also measured, respectively (Fig. S7). Compared to the FT-IR spectra of **L**, the characteristic OH absorption peak at 3346 cm^{-1} vanished in the presence of Al^{3+} , indicating the deprotonation of phenolic hydroxyl and the coordination of oxygen atom with the Al^{3+} ion. The characteristic imide absorption of linker $-\text{C}=\text{N}-$ shifted from 1593 cm^{-1} to 1373 cm^{-1} , which is accordance with previous reports [8]. This variation could be caused by the coordination of the imide N atom to the Al^{3+} ions.

^1H NMR experiments were carried out in DMSO d_6 to understand the exact binding mode of **L**- Al^{3+} . As show in Fig. 9, upon the addition of Al^{3+} , the protons of hydroxyl (H_a) and of amide (H_j) connected with quinoline ring of **L** were all disappeared, indicated the occurrence of deprotonation during the process of coordination of Al^{3+} with oxygen atom of the hydroxyl and the nitrogen of amide. In addition, the protons of methylene (H_d and H_g) and the protons (H_e and H_f) of the piperazine moiety **L** were all obviously shifted downfield to 3.39 ppm, indicating that the two nitrogen atoms of piperazine ring might coordinate to Al^{3+} .

According to the analysis of Job's plot, ESI-MS, FT-IR spectra and ^1H NMR, a possible bonding mode for **L** with Al^{3+} was proposed (Scheme 3).

3.4. Effect of pH Toward the Fluorescence Intensity

In order to evaluate the practical applicability, the effect of pH on the emission intensity ($\lambda_{\text{em}} = 440 \text{ nm}$) of **L** in the absence and presence of Al^{3+} were measured, respectively (Fig. S8). The probe **L** has almost no fluorescence emission in the wide pH range 2–12, but upon addition of Al^{3+} into **L** at different pH conditions, obvious fluorescence enhancement was observed from pH 4 to 8, indicated

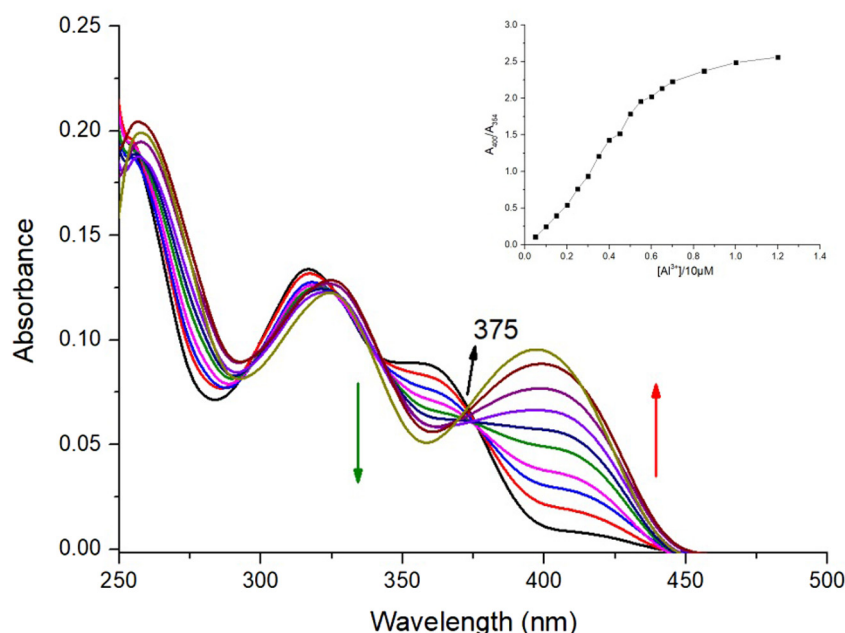


Fig. 6. UV-vis absorption spectra of **L** (10 μM) in DMF/ H_2O (1/9, v/v) upon the addition of Al^{3+} (0–12 μM).

Table 1
Comparison of the characteristics of **L** with the previously reported Al³⁺ sensors.

Ref.	Methods of detections	Selectivity	Interfering metal ions	LOD	Binding constants	Recovery
[29]	Ratiometric fluorescent	Al ³⁺	NR	2.9 × 10 ⁻⁷ M	NR	NR
[30]	Ratiometric fluorescent	Al ³⁺	None	2.9 × 10 ⁻⁷ M	NR	EDTA ²⁻
[31]	Fluorescent	Al ³⁺	Cu ²⁺	4 × 10 ⁻⁶ M	4 × 10 ³ M ⁻¹	EDTA ²⁻
[32]	Ratiometric fluorescent	Al ³⁺	None	2.4 × 10 ⁻⁸ M	5.6 × 10 ⁴ M ⁻¹	NR
[33]	Ratiometric fluorescent	Al ³⁺ 、Fe ³⁺ 、Cr ³⁺	None	2.3 × 10 ⁻⁵ M	8.77 × 10 ³ M ⁻¹	NR
[34]	Absorbance	Al ³⁺ 、Fe ³⁺ 、Cr ³⁺	None	7.79 × 10 ⁻⁸ M	6.7 × 10 ⁴ M ⁻¹	NR
	Ratiometric fluorescent			2.71 × 10 ⁻⁸ M		
[35]	Colorimetric and ratiometric fluorescent	Al ³⁺	Ni ²⁺ and Cu ²⁺	5.21 × 10 ⁻⁷ M	2.08 × 10 ⁶ M ⁻²	NR
[36]	Ratiometric fluorescent	Al ³⁺	None	8.06 × 10 ⁻⁸ M	2.31 × 10 ⁴ M ⁻¹	NR
[37]	Colorimetric and fluorescent	Al ³⁺	None	1.59 × 10 ⁻⁷ M	6.37 × 10 ⁴ M ⁻¹	EDTA ²⁻
[38]	Colorimetric and fluorescent	Al ³⁺	Mn ²⁺	6.9 × 10 ⁻⁶ M	7.6 × 10 ⁴ M ⁻¹	EDTA ²⁻
[39]	Colorimetric and fluorescent	Al ³⁺	None	7.4 × 10 ⁻⁹ M	1.62 × 10 ⁴ M ⁻¹	NR
This work	Ratiometric absorbance	Al ³⁺	Cu ²⁺	3.67 × 10 ⁻⁸ M	6.6 × 10 ⁴ M ⁻¹	EDTA ²⁻
	Fluorescent			1.92 × 10 ⁻⁷ M	1.038 × 10 ⁴ M ⁻¹	

LOD: The limit of detection; NR: Not reported in the corresponding paper.

that **L** could be a good probe for Al³⁺ detection in neutral to acidic medium.

3.5. Reversibility of **L** for Al³⁺

Reversibility is another significant criterion for the development of chemosensor in the facet of its practical application. The reversibility of the recognition process of **L** was investigated by adding Na₂EDTA which is a common binding agent for Al³⁺ (Fig. S9–S10). Upon the addition of Al³⁺, the absorption band of **L** at 354 nm disappeared and a new band at 400 nm emerged, and the dramatic fluorescence enhancement at 440 nm also was observed in its fluorescence spectrum. However, the addition of EDTA to the solutions of **L**-Al³⁺, the UV-Vis absorption spectra and fluorescence spectra of the solution of **L**-Al³⁺ were all nearly recovered to the original state of **L** in the absence of Al³⁺, indicating the regeneration of the **L**. Such reversibility and regeneration are significant for the manufacture of devices to detect Al³⁺.

3.6. Application of **L** for Al³⁺ Analysis in Water Samples

In order to explore the practical application of **L** for the detection of aluminum ions, detail experiments were carried out for the

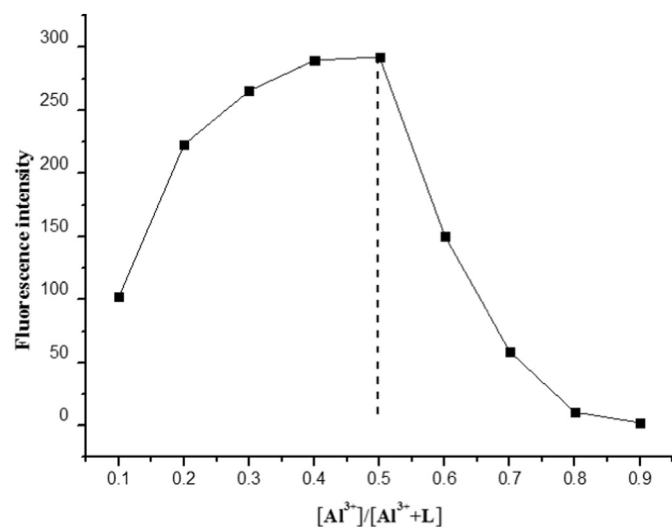


Fig. 7. Job plot of Al³⁺ complex formation. $\{[Al^{3+}] / ([Al^{3+}] + [L])\}$ is the molar fraction of Al³⁺ ion.

determination of Al³⁺ in real water samples collected from local region of campus. Water samples were spiked with standard Al³⁺ ions at different concentration levels, and then diluted within working linear range and analyzed with the method proposed under optimized conditions (Table 2). The results show that **L** has good recoverability and high accuracy for the practical application of aluminum ions in water, indicated that **L** could be used in Al³⁺ detection in environmental analysis.

3.7. Molecular Logic Gates

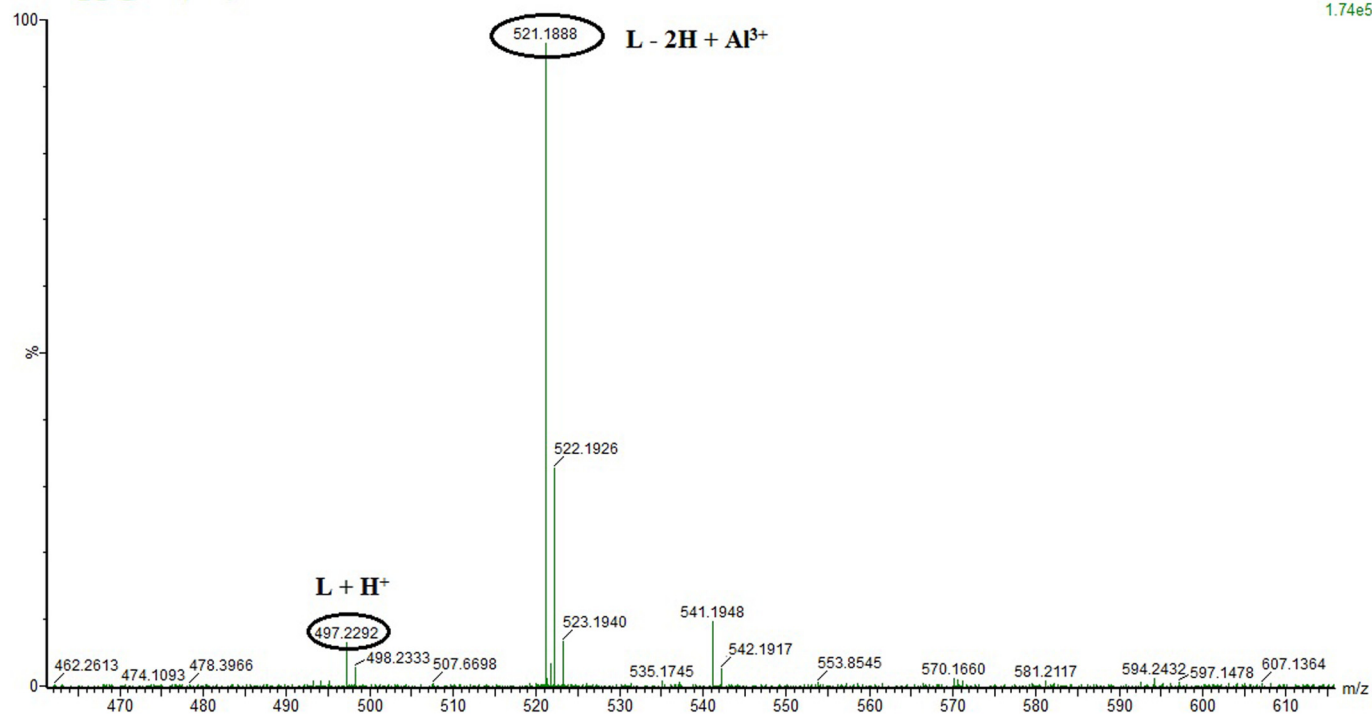
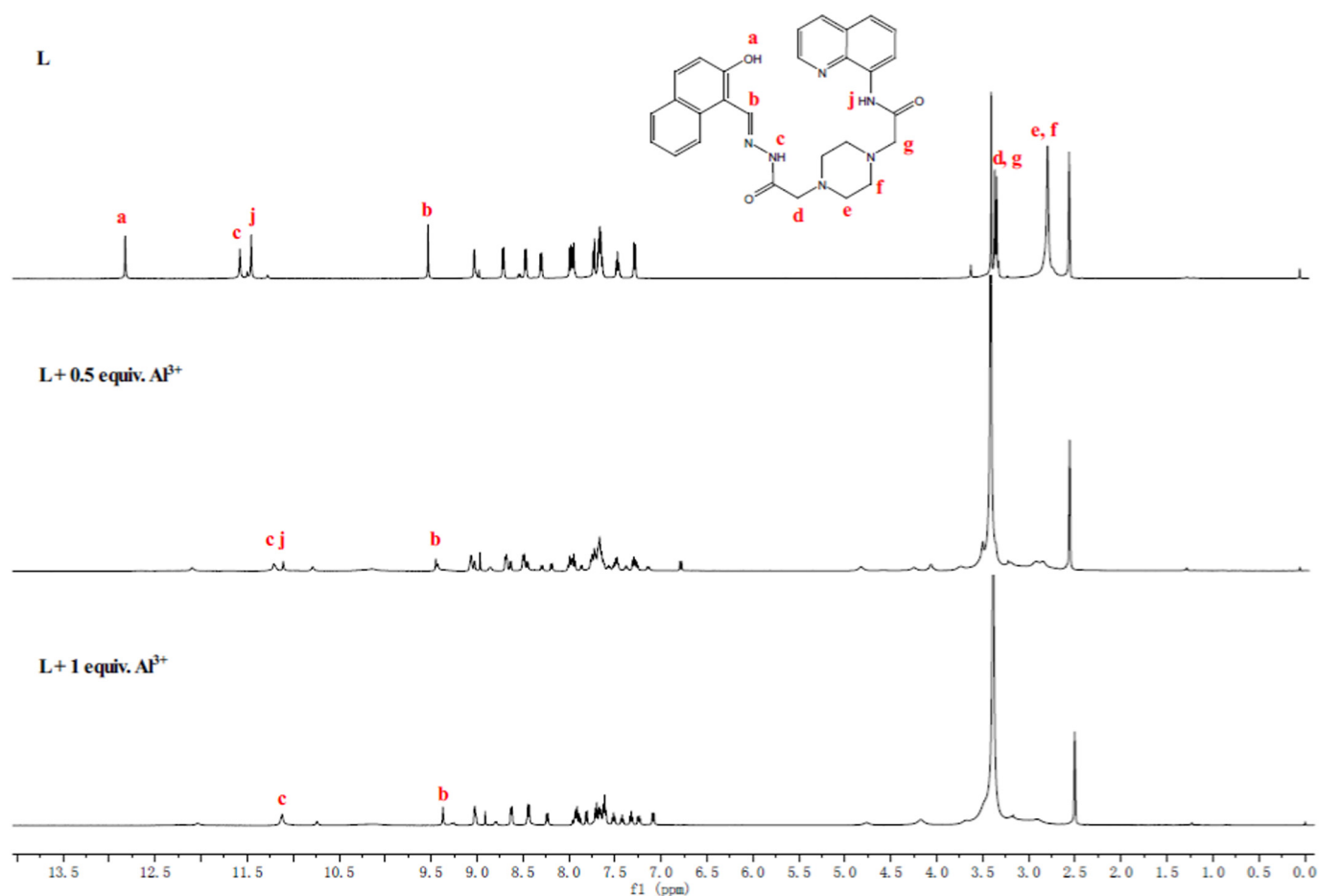
One major feature of information technology is the processing of input signals by logic gates [45]. In today's era, molecular logic gates become increasingly important in the field of molecular computing research. Thus, based on the fluorescence responses of **L** with Al³⁺ and EDTA, one identical molecular logic gate has been designed, which is a INHIBIT logic gate (Fig. 10).

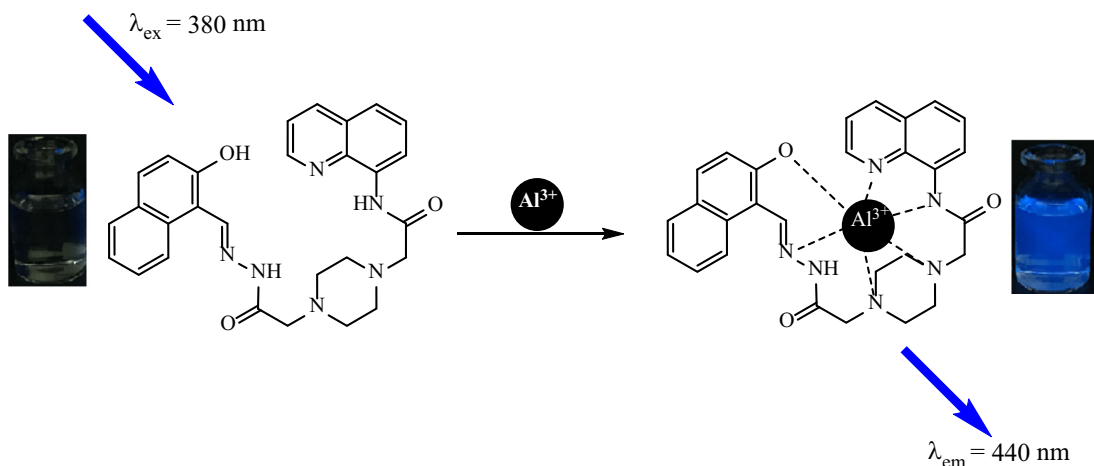
We set Al³⁺ and EDTA separately as inputs signals 1 and inputs signals 2 for the Set (S) and Reset I process, the fluorescence signal of the chemosensor **L** at 440 nm as output. In truth table shown in Fig. 10, the fluorescence intensity is low for Off (0) state and high for On (1) state. When neither input is on, the gate is off. When only input 1 (Al³⁺) is present, the chemosensor showed a significant fluorescence enhancement at 440 nm and indicating ON state of the system. When only input 2 (EDTA) is present, the emission is low at this output indicating OFF state. When both the inputs are present, the output is also in the off condition. Based on the above basic logic gates, a sequential logic circuit i.e. memory device which displays “write-read-erase-read” sequences in the form of binary logic function can be constructed [8]. Now the system writes the state “1” when the SET input is high at 440 nm and it is erased by RESET input resulting in state “0”. And this form of setting can cause the entire process to be repeated several times. However, according to the result of the competitive experiment, this molecular logic gates has its limitation in that it is not able to confirm whether the existence of Al³⁺ in tested sample which had been contaminated with Cu²⁺.

3.8. Cells Imaging

For evaluation of the potential of detecting Al³⁺ in cells with **L**, the human stromal cell (HSC), this endometrium fibroblast cell line was derived from the human stromal cells and immortalized with hTERT, has been used as an *in vitro* model. Chemically defined serum-free and antibiotic-free medium was used to incubate cells with chemical for avoid non-specific fluorescence. As determined by laser confocal microscope (Fig. 11), the cells without Al³⁺-loading gave no intracellular fluorescence. After the cells was incubated with **L** in the presence of

20170320_L_30_AI 301 (0.669)

1: TOF MS ES+
1.74e5Fig. 8. ESI-MS spectrum of L (50 μM) upon addition of 5 equiv. of Al^{3+} in $\text{CH}_3\text{CH}_2\text{OH}$.Fig. 9. ^1H NMR spectra of L with Al^{3+} in $\text{DMSO } d_6$.



Scheme 3. Probable binding mode of sensor **L** with Al^{3+} ions.

Table 2
Determination of Al^{3+} in water samples from different water sources.

Water samples studied	Amount of standard Al^{3+} added ($\mu\text{mol/L}$)	Total Al^{3+} found ($n = 3$) ($\mu\text{mol/L}$)	Recovery of Al^{3+} ($n = 3$) added (%)	RSD (%)	Relative error (%)
Ultrapure water	3	2.96	98.67	1.02	-1.30
	5	4.84	96.80	2.13	-3.20
	6	6.15	102.50	4.54	2.50
Tap water (Department of Chemistry)	3	2.96	98.67	0.90	-1.33
	5	5.21	104.20	2.09	4.20
	6	6.16	102.67	2.89	2.67

4. Conclusion

In summary, we successfully designed and synthesized a highly selective and sensitive chemosensor **L** through distinct fluorescence enhancement (335-fold) and ratiometric detection Al^{3+} in DMF/ H_2O (v/v, 1/9) based on the combined mechanisms of ESIPT and CHEF. The binding phenomenon of **L** and Al^{3+} was successfully studied by different spectroscopic techniques, and the limit of detection for Al^{3+} was determined as 3.67×10^{-8} M. Moreover, **L** was successfully applied for the detection of Al^{3+} in cells HSC confirming its low cytotoxicity and good imaging characteristics.

Acknowledgements

This work was supported by the Scientific Research Fund of Heilongjiang Provincial Education Department (No. 12531033).

different amounts of Al^{3+} (5 and 50 μM), the cells showed a strong fluorescent. These results suggest that the probe **L** have potential biomedical applications.

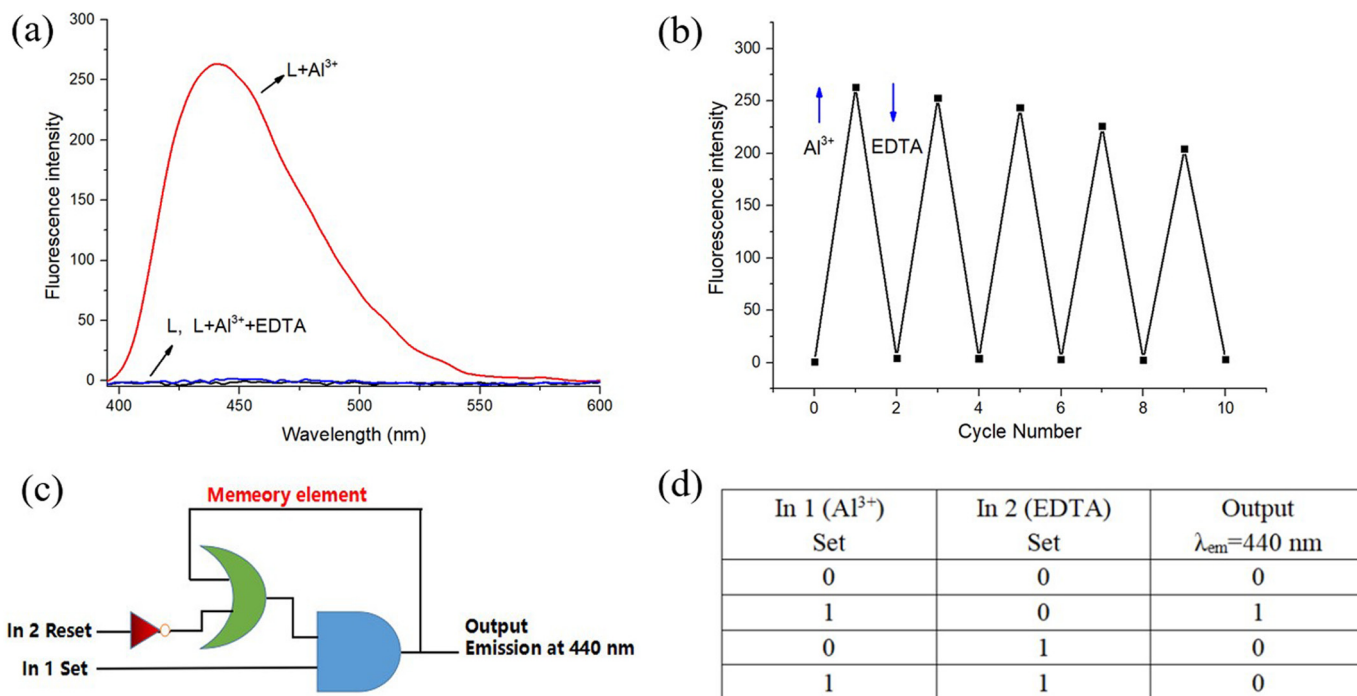


Fig. 10. (a) INHIBIT logic gates based on **L** by monitoring of the emission spectral change at 440 nm in the presence of Al^{3+} (5 equiv.) and EDTA (5 equiv.); (b) fluorescence intensity changes of **L** at 440 nm upon alternate addition of Al^{3+} and EDTA for five cycles; (c) the logic circuit displaying memory unit with two inputs (In 1 and In 2) and one output, and (d) corresponding truth table.

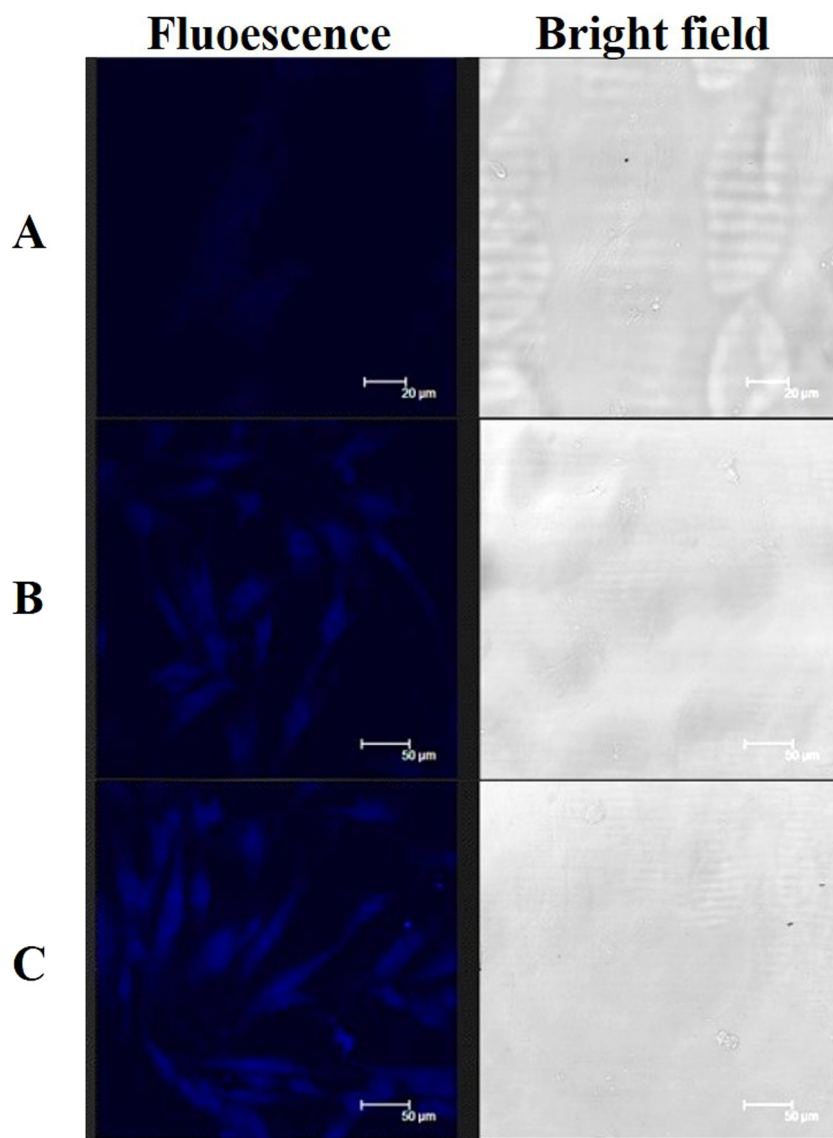


Fig. 11. (A) The cells was incubated 2 h with **L** (0.1 mM); (B) cells was incubated 5 μM of Al^{3+} and 0.1 mM of **L**; (C) cells was incubated 50 μM of Al^{3+} and 0.1 mM of **L**.

Appendix A. Supplementary data

Supplementary data to this article can be found online at <https://doi.org/10.1016/j.saa.2018.07.039>.

References

- [1] R. Azadbakht, M. Talebi, J. Karimi, R. Golbedaghi, Synthesis and characterization of a new organic nanoparticle as fluorescent chemosensor for aluminum ions, *Inorg. Chim. Acta* 453 (2016) 728–734.
- [2] R. Wang, G.Q. Jiang, X.H. Li, Two 5, 5'-methylenebis(salicylaldehyde)-based Schiff base fluorescent sensors for selective sensing of Al^{3+} in DMSO/ H_2O solution, *Inorg. Chim. Acta* 455 (2017) 247–253.
- [3] U. Panda, S. Roy, D. Mallick, A. Layek, P.P. Ray, C. Sinha, Aggregation induced emission enhancement (AIEE) of fluorenyl appended Schiff base: a turn on fluorescent probe for Al^{3+} , and its photovoltaic effect, *J. Lumin.* 181 (2017) 56–62.
- [4] Y.S. Dong, T.Q. Liu, X.J. Wan, H. Pei, L.S. Wu, Y.W. Yao, Facile one-pot synthesis of bipyridine-based dual-channel chemosensor for the highly selective and sensitive detection of aluminum ion, *Sensors Actuators B Chem.* 241 (2017) 1139–1144.
- [5] F. Wang, Y.L. Xu, S.O. Aderinto, H.P. Peng, H. Zhang, H.L. Wu, A new highly effective fluorescent probe for Al^{3+} ions and its application in practical samples, *J. Photochem. Photobiol. A Chem.* 332 (2017) 273–282.
- [6] L.J. Tang, S.L. Ding, K.L. Zhong, S.H. Hou, Y.J. Bian, X.M. Yan, A new 2-(2'-hydroxyphenyl)quinazolin-4(3H)-one derived acylhydrazone for fluorescence recognition of Al^{3+} , *Spectrochim. Acta A* 174 (2017) 70–74.
- [7] D. Don, K. Velmurugan, J. Prabhu, N. Bhuvanesh, A. Thamilselvan, R. Nandhakumar, A dual analyte fluorescent chemosensor based on a furan-pyrene conjugate for Al^{3+} & HSO_3^- , *Spectrochim. Acta A* 174 (2017) 62–69.
- [8] A. Roy, S. Dey, P. Roy, A ratiometric chemosensor for Al^{3+} based on naphthalene-quinoline conjugate with the resultant complex as secondary sensor for F^- : interpretation of molecular logic gates, *Sensors Actuators B Chem.* 237 (2016) 628–642.
- [9] B. Liu, P.F. Wang, J. Chai, X.Q. Hu, T. Gao, J.B. Chao, T.G. Chen, B.S. Yang, Naphthol-based fluorescent sensors for aluminium ion and application to bioimaging, *Spectrochim. Acta A* 168 (2016) 98–103.
- [10] T.G. Jo, K.H. Bok, J. Han, M.H. Lim, C. Kim, Colorimetric detection of Fe^{3+} and Fe^{2+} and sequential fluorescent detection of Al^{3+} and pyrophosphate by an imidazole-based chemosensor in a near-perfect aqueous solution, *Dyes Pigments* 139 (2017) 136–147.
- [11] G.T. Selvan, M. Kumaresan, R. Sivaraj, I.V.M.V. Enoch, P.M. Selvakumar, Isomeric 4-aminoantipyrine derivatives as fluorescent chemosensors of Al^{3+} ions and their molecular logic behaviour, *Sensors Actuators B Chem.* 229 (2016) 181–189.
- [12] S.M. Hossain, K. Singh, A. Lakma, R.N. Pradhan, A.K. Singh, A schiff base ligand of coumarin derivative as an ICT-based fluorescence chemosensor for Al^{3+} , *Sensors Actuators B Chem.* 239 (2017) 1109–1117.
- [13] E. Delhaize, P.R. Ryan, Aluminum toxicity and tolerance in plants, *Plant Physiol.* 107 (1995) 315–321.
- [14] F.U. Rahman, A. Ali, S.K. Khalil, R. Guo, P. Zhang, H. Wang, Z.T. Li, D.W. Zhang, Tuning sensitivity of a simple hydrazone for selective fluorescent “turn on” chemo-sensing of Al^{3+} and its application in living cells imaging, *Talanta* 164 (2017) 307–313.
- [15] H.Y. Jeong, S.Y. Lee, J. Han, M.H. Lim, C. Kim, Thiophene and diethylaminophenol-based “turn-on” fluorescence chemosensor for detection of Al^{3+} and F^- in a near-perfect aqueous solution, *Tetrahedron* 73 (2017) 2690–2697.

- [16] E.T. Feng, R.M. Lu, C.B. Fan, C.H. Zheng, S.Z. Pu, A fluorescent sensor for Al^{3+} based on a photochromic diarylethene with a hydrazinobenzothiazole Schiff base unit, *Tetrahedron Lett.* 58 (2017) 1390–1394.
- [17] Y.J. Liu, F.F. Tian, X.Y. Fan, F.L. Jiang, Y. Liu, Fabrication of an acylhydrazone based fluorescence probe for Al^{3+} , *Sensors Actuators B Chem.* 240 (2017) 916–925.
- [18] L.K. Kumawat, N. Mergu, M. Asif, V.K. Gupta, Novel synthesized antipyrine derivative based “naked eye” colorimetric chemosensors for Al^{3+} and Cr^{3+} , *Sensors Actuators B Chem.* 231 (2016) 847–859.
- [19] D. Sarkar, P. Ghosh, S. Gharami, T.K. Mondal, N. Murmu, A novel coumarin based molecular switch for the sequential detection of Al^{3+} and F^- : application in lung cancer live cell imaging and construction of logic gate, *Sensors Actuators B Chem.* 242 (2017) 338–346.
- [20] S.Z. Pu, C.C. Zhang, C.B. Fan, G. Liu, Multi-controllable properties of an antipyrine-based diarylethene and its high selectivity for recognition of Al^{3+} , *Dyes Pigments* 129 (2016) 24–33.
- [21] L.J. Tang, X. Dai, X. Wen, D. Wu, Q. Zhang, A rhodamine–benzothiazole conjugated sensor for colorimetric, ratiometric and sequential recognition of copper(II) and sulfide in aqueous media, *Spectrochim. Acta A* 139 (2015) 329–334.
- [22] T.T. Chen, T.W. Wei, Z.J. Zhang, Y.H. Chen, J. Qiang, F. Wang, X.Q. Chen, Highly sensitive and selective ESIPT-based fluorescent probes for detection of Pd^{2+} with large Stokes shifts, *Dyes Pigments* 140 (2017) 392–398.
- [23] S. Banerjee, P. Brandao, A. Saha, A robust fluorescent chemosensor for aluminium ion detection based on a Schiff base ligand with an azo arm and application in a molecular logic gate, *RSC Adv.* 6 (2016) 101924–101936.
- [24] C.R. Li, S.L. Li, Z.Y. Yang, A chromone-derived Schiff-base as Al^{3+} “turn-on” fluorescent probe based on photoinduced electron-transfer (PET) and C=N isomerization, *Tetrahedron Lett.* 57 (2016) 4898–4904.
- [25] M. Maniyazagan, R. Mariadasse, M. Nachiappan, J. Jeyakanthan, N.K. Lokanath, S. Naveen, G. Sivaraman, P. Muthuraja, P. Manisankar, T. Stalin, Synthesis of rhodamine based organic nanorods for efficient chemosensor probe for Al (III) ions and its biological applications, *Sensors Actuators B Chem.* 254 (2018) 795–804.
- [26] P. Torawane, K. Tayade, S. Bothra, S.K. Sahoo, N. Singh, A. Borse, A. Kuwar, A highly selective and sensitive fluorescent ‘turn-on’ chemosensor for Al^{3+} based on C=N isomerisation mechanism with nanomolar detection, *Sensors Actuators B Chem.* 222 (2016) 562–566.
- [27] X. Hu, X.X. Mao, X.D. Zhang, Y.M. Huang, One-step synthesis of orange fluorescent copper nanoclusters for sensitive and selective sensing of Al^{3+} ions in food samples, *Sensors Actuators B Chem.* 247 (2017) 312–318.
- [28] N. Xiao, L.L. Xie, X.M. Zhi, C.J. Fang, A naphthol-based highly selective fluorescence turn-on and reversible sensor for Al(III) ion, *Inorg. Chem. Commun.* 89 (2018) 13–17.
- [29] L. Peng, Z.J. Zhou, X.Y. Wang, R.R. Wei, K. Li, Y. Xiang, A.J. Tong, A ratiometric fluorescent chemosensor for Al^{3+} in aqueous solution based on aggregation-induced emission and its application in live-cell imaging, *Anal. Chim. Acta* 829 (2014) 54–59.
- [30] H.T. Xie, Y.L. Wu, J. Huang, F. Zeng, H. Wu, X.T. Xia, C.M. Yu, S.Z. Wu, A ratiometric fluorescent probe for aluminum ions based-on monomer/excimer conversion and its applications to real sample, *Talanta* 151 (2016) 8–13.
- [31] J.C. Qin, Z.Y. Yang, P. Yang, Recognition of Al^{3+} based on a naphthalene-based “Off-On” chemosensor in near 100% aqueous media, *Inorg. Chim. Acta* 432 (2015) 136–141.
- [32] Q. Zhu, L. Li, L. Mu, X. Zeng, C. Redshaw, G. Wei, A ratiometric Al^{3+} ion probe based on the coumarin–quinoline FRET system, *J. Photochem. Photobiol. A Chem.* 328 (2016) 217–224.
- [33] S. Goswami, K. Aich, A.K. Das, A. Manna, S. Das, A naphthalimide–quinoline based probe for selective, fluorescence ratiometric sensing of trivalent ions, *RSC Adv.* 3 (2013) 2412–2416.
- [34] N.R. Chereddy, M.V.N. Raju, B.M. Reddy, V.R. Krishnaswamy, P.S. Korrapati, B.J.M. Reddy, V.J. Rao, A TBET based BODIPY–rhodamine dyad for the ratiometric detection of trivalent metal ions and its application in live cell imaging, *Sensors Actuators B Chem.* 237 (2016) 605–612.
- [35] P.J. Hung, J.L. Chir, W. Ting, A.T. Wu, A selective colorimetric and ratiometric fluorescent chemosensor for detection of Al^{3+} ion, *J. Lumin.* 158 (2015) 371–375.
- [36] J.C. Qin, J. Yan, B.D. Wang, Z.Y. Yang, Rhodamine–naphthalene conjugate as a novel ratiometric fluorescent probe for recognition of Al^{3+} , *Tetrahedron Lett.* 57 (2016) 1935–1939.
- [37] N.N. Li, S. Zeng, M.Q. Li, Y.Q. Ma, X.J. Sun, Z.Y. Xing, J.L. Li, A highly selective naphthalimide-based chemosensor: “naked-eye” colorimetric and fluorescent turn-on recognition of Al^{3+} and its application in practical samples, test paper and logic gate, *J. Fluoresc.* 28 (2018) 347–357.
- [38] L. Kang, Z.Y. Xing, X.Y. Ma, Y.T. Liu, Y. Zhang, A highly selective colorimetric and fluorescent turn-on chemosensor for Al^{3+} based on naphthalimide derivative, *Spectrochim. Acta A* 167 (2016) 59–65.
- [39] L. Kang, Y.T. Liu, N.N. Li, Q.X. Dang, Z.Y. Xing, J.L. Li, Y. Zhang, A schiff-base receptor based naphthalimide derivative: highly selective and colorimetric fluorescent turn-on sensor for Al^{3+} , *J. Lumin.* 186 (2017) 48–52.
- [40] Y. Zhang, X.F. Guo, W.X. Si, L.H. Jia, X.H. Qian, Ratiometric and water-soluble fluorescent zinc sensor of carboxamidoquinoline with an alkoxyethylamino chain as receptor, *Org. Lett.* 10 (2008) 473–476.
- [41] N.N. Li, Y.Q. Ma, S. Zeng, Y.T. Liu, X.J. Sun, Z.Y. Xing, A highly selective colorimetric and fluorescent turn-on chemosensor for Zn^{2+} and its logic gate behavior, *Synth. Met.* 232 (2017) 17–24.
- [42] M. Kumar, A. Kumar, M.S.H. Faizi, S. Kumar, M.K. Singh, S.K. Sahu, S. Kishor, R.P. John, A selective ‘turn-on’ fluorescent chemosensor for detection of Al^{3+} in aqueous medium: experimental and theoretical studies, *Sensors Actuators B Chem.* 260 (2018) 888–899.
- [43] Y.W. Huang, Q. Lin, J.M. Wu, N.Y. Fu, Design and synthesis of a squaraine based near-infrared fluorescent probe for the ratiometric detection of Zn^{2+} ions, *Dyes Pigments* 99 (2013) 699–704.
- [44] H.Y. Liu, B.B. Zhang, C.Y. Tan, F. Liu, J.K. Cao, Y. Tan, Y.Y. Jiang, Simultaneous bioimaging recognition of Al^{3+} and Cu^{2+} in living-cell, and further detection of F^- and S^{2-} by a simple fluorogenic benzimidazole-based chemosensor, *Talanta* 161 (2016) 309–319.
- [45] P. Ball, Chemistry meets computing, *Nature* 406 (2000) 118–120.